The Complex Subband Decomposition and its Application to the Decimation of Large Adaptive Filtering Problems

James P. Reilly*, Matt Wilbur, Michael Seibert and Nima Ahmadvand
The Department of Electrical and Computer Engineering
McMaster University, Hamilton, Ontario, Canada L8S 4K1
EDICS: 2-MWAV

Submitted for publication in IEEE Transactions on Signal Processing

Abstract

In this paper, we show that an NPR M-channel filter bank with a diagonal system inserted between the analysis and synthesis filter banks may be used to decompose an FIR system of order L into M complex subband components each of order $\frac{L}{K}$, where K is the downsampling rate. This decomposition is at the expense of using complex arithmetic for the subband processing.

The theory surrounding the proposed filter bank structure leads to a new understanding of subbanded adaptive filtering implementations. It also leads naturally to a *delayless* subbanded adaptive filter scheme.

Using conditions on the analysis and synthesis filters, the formulas for the subband components and their respective properties are developed. Simulation results for an acoustic echo cancellation example are given to support the developed theory.

*J. Reilly (corresponding author) ph: 905 525 9140 x22895, fax: 905 521 2922, email: reillyj@mcmaster.ca

1 Introduction

Filter bank theory [1] is by now a mature topic. The classical approach to this subject has concentrated on the development of perfect reconstruction (PR) or near perfect reconstruction (NPR) filter bank systems, salient features of which are that the overall frequency response of the filter bank is distortionless, and that the aliasing error introduced from downsampling in the subbands is cancelled at the output. This theory requires that there be no processing in the subbands. This requirement has limited the application of filter bank theory to such areas as data compression and related topics.

In this paper, we show that a *diagonal* $M \times M$ system $\mathbf{C}(z)$ can indeed be inserted between the analysis and synthesis filters of an M–channel filter bank in a meaningful way. By this, we mean that an arbitrary FIR system $S(z)$ of order L (which may be large) can be decimated by a filter bank structure shown in Figure 1 where the subband components $C_m(z)$ of $\mathbf{C}(z)$ are each of order $O(\frac{L}{K})$, where K is the downsampling rate of the filter bank. In the approach adopted in this paper, the analysis and synthesis filters have single-sided frequency responses.

This decimation can render computationally intractable problems feasible, and is useful in applications such as audio and acoustics, which typically involve determination of a very large number of parameters describing an acoustic channel. Examples include blind identification of room impulse responses [2], adaptive beamforming [3], and active noise control [4]. In this paper however, we concentrate on the acoustic echo cancellation (AEC) problem in telephony. This problem is associated with the hands–free telephone, which requires an acoustic echo canceller to eliminate the acoustic feedback from the loudspeaker, through the room, and back to the microphone. This device is an adaptive filter which estimates the acoustic impulse response (AIR) of the room and uses this estimate to suppress the echo signal which is picked up by the microphone and sent back to the far end. The difficulty with this particular application is that the AIR is very long (typically on the order of several thousand samples) and the required adaptation rate is very fast, due to the rate at which the acoustic properties of the room can change. The implementation must also be very inexpensive. This later requirement stipulates the use of the LMS algorithm, but its performance is typically not adequate in these adverse circumstances.

The classical filter bank theory has recently been extended through the use of subbanded adaptive filters [5] – [11], which have proven very successful in the AEC application. Subbanding using the single–sided filter bank approach proposed here has been used previously for adaptive filtering [10] and for transmultiplexing [12][13]. However, the concept of subbanded adaptive filtering has generally evolved from an *ad hoc* motivation, despite the fact it has been well researched. In this paper, we present new theoretical results using single–sided filter banks which rigorously justify subband adaptive filtering.

One of the difficulties associated with a subbanded approach to the AEC problem is filter bank delay. Excessive delay in the speech path leads to difficulty in conducting a natural, full-duplex conversation. Thus there have been *delayless* subbanded methods proposed [14][15][16]. The theo-

retical development presented in this paper leads naturally to a delayless adaptive filter structure, which is similar to that presented in [14]. The proposed method is briefly discussed in this paper.

In Section 2, we show that aliasing in the subbands can be (approximately) eliminated through the use of filter banks with single–sided[1] frequency responses. We then show this property permits the system $\mathbf{C}(z)$ to be *diagonal*. In contrast, for the general case, the system $\mathbf{C}(z)$ must be considered a dense $M \times M$ matrix in order to completely suppress aliasing errors [5][6]. We then show that a sequence of M subband components $C_m(z)$ can approximate an arbitrary LTI system $S(z)$ of interest. A straightforward method of identifying the subband components is then presented and it is shown that the subband components are indeed of order $\frac{L}{K}$. We show there exists a many–to–one correspondence between the subband components and the model response $S(z)$. We also show that convolution inside the subbands of the subband components representing two signals of interest, is approximately equivalent to the convolution outside the subbands of the signals themselves. The delayless adaptive filter implementation is briefly discussed. These theoretical insights offer new approaches and flexibility for implementation of adaptive filtering problems.

In Section 3, we briefly discuss procedures for the design of the analysis and synthesis filters. Verification of the theory and simulations of the AEC problem are presented in Section 4. Conclusions are then presented in Section 5.

Notation: We use non–bold upper–case characters to denote a polynomial in z: e.g. $X(z)$. The lower–case version of the symbol, e.g., $x[n]$ represents the corresponding sequence in time. A bold lower–case character, e.g., $\mathbf{x}(z)$ and a bold upper–case upper case character, e.g., $\mathbf{H}(z)$ represent a vector and a matrix respectively, whose elements are polynomials in z. A bold lower–case character without a z–argument ($\mathbf{x}$) represents a vector whose elements define a sequence in time. The superscript ^{T} represents the transpose operation. The notation $[\cdot]_{\downarrow K}$ means the argument has been downsampled by a factor of K.

2 The Complex Subband Decomposition

In this section, we develop the complex subband decomposition of an arbitrary LTI system $S(z)$ shown in Figure 1a, using the oversampled M–channel filter bank shown in Figure 1b.

[1]This term follows from the term "single sideband modulation". Here, we retain e.g., the positive frequency components corresponding to a real signal, and suppress the negative components.

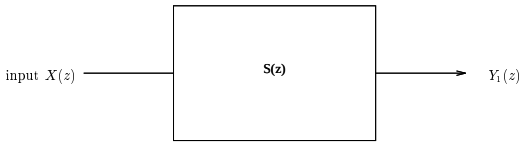

(a)

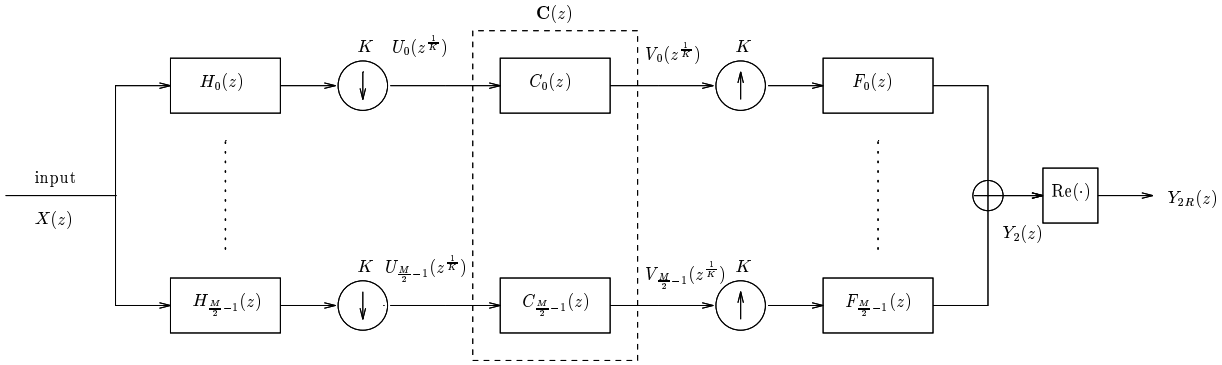

(b)

Figure 1: (a) An arbitary FIR system $S(z)$. (b) A subband approximation of the system $S(z)$.

2.1 Complex Filter banks

To begin, we define a set of M overlapping frequency bands Ω_M^m over the range $0 \leq \omega \leq 2\pi$ such that

$$\Omega_M^m = \left\{ \omega : \frac{2\pi m}{M} - \epsilon \leq \omega < \frac{2\pi(m+1)}{M} + \epsilon \right\}, \qquad m = 0, 1, \ldots, M-1, \tag{1}$$

where ϵ is a transition bandwidth corresponding to a practical analysis filter response. The integer M is taken to be even.

Consider a set of FIR analysis filters of Figure 1b, each of length N, having *single-sided* frequency responses $H_m(z), m = 0 \ldots, M-1$, with the response specification

$$\left| H_m(z) \right|_{z=e^{j\omega}} \approx \begin{cases} \text{finite magnitude}, & \omega \in \Omega_M^m \\ 0, & \text{otherwise}, \end{cases} \tag{2}$$

as shown in Figure 2a. These filters are related in the time domain to a real low pass prototype with cutoff frequency $\frac{\pi}{M}$ as shown in Figure 2b, by

$$h_m[n] = h_{pr}[n] e^{j\frac{2\pi}{M}(m+m_0)(n+n_0)}. \tag{3}$$

For the filter bank under discussion, we make the following set of assumptions: a) $f_{pr}[n] = h_{pr}[N - n]$, b) $f_m[n] = f_{pr}[n]e^{j\frac{2\pi}{M}(m-m_0)(n+n_0)}$, and c) $m_0 = \frac{1}{2}$ and $n_0 = 0$. Under these assumptions, the z-domain version of (3) is

$$H_m(z) = H_{pr}(zW_M^{-(m+\frac{1}{2})}) \tag{4}$$

where $W_M^m = e^{-j2\pi\frac{m}{M}}$. Similarly, for the synthesis filters we have

$$F_m(z) = F_{pr}(zW_M^{-(m+\frac{1}{2})}). \tag{5}$$

We further assume the input signal $x[n]$ and the model response $s[n]$ are real.

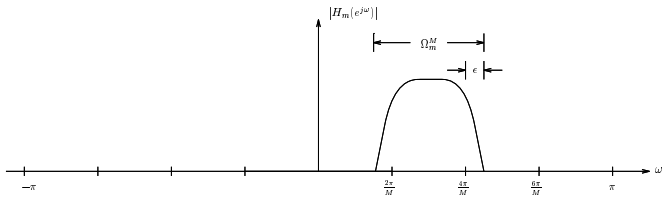

(a)

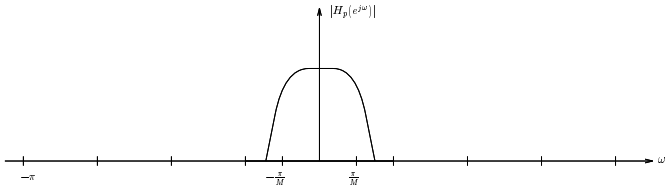

(b)

Figure 2: (a) Example of the magnitude response of $H_1(z)$. (b) Corresponding prototype filter $H_p(e^{j\omega})$

The analysis and synthesis filters are designed so that the filter bank satisfies the following properties, which we show later to be sufficient for the subband structure of Figure 1b to represent the system $S(z)$, for appropriately chosen $\mathbf{C}(z)$:

1.

$$F_m(z)H_m(zW_K^k)|_{z=e^{j\omega}} \approx 0 \qquad \begin{cases} k = 1, \ldots, K-1 \\ m = 0, \ldots, \frac{M}{2} - 1 \\ 0 \le \omega < 2\pi, \end{cases} \tag{6}$$

2.

$$\frac{1}{2}\left[\sum_{m=0}^{\frac{M}{2}-1} F_m(z)H_m(z) + F_m^*(z)H_m^*(z)\right] \approx dz^{-k_0} \tag{7}$$

where * denotes complex conjugation, d is a constant and k_0 is a delay introduced for causality[2]. The inclusion of the second term above is equivalent to taking the real part in the time domain as shown at the output of Figure 1b.

Equation (6) can be satisfied by making K not too large with respect to M. Eq. (7) can be satisfied by making $H_{pr}(z)$ a root-Nyquist filter.

Figure 3 shows an example of $H_0(z)$ resulting from downsampling then upsampling by a factor of K. From this figure, it is clear that (6) can only be satisfied if the shift $\frac{2\pi}{K}$ is greater than the bandwidth occupied by Ω_M^m; i.e.,

$$\frac{2\pi}{M} + 2\epsilon \leq \frac{2\pi}{K}. \tag{8}$$

or

$$K < \frac{M}{1 + \frac{\epsilon M}{\pi}}. \tag{9}$$

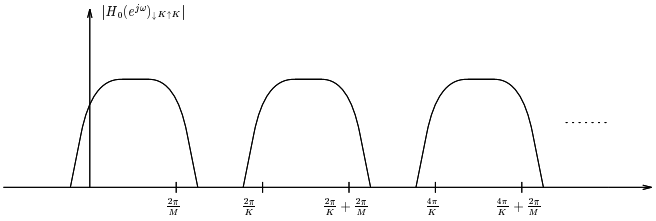

Figure 3: The magnitude spectrum $H_0(e^{j\omega})$ after downsampling and upsampling by a factor of K.

In the sequel, we shall refer to an "ideal" prototype filter. By this, we mean that the prototype $H_{pr}(z)$ is such that (6) and (7) are satisfied with equality.

Note that a necessary condition for (6) is that the frequency responses $H_m(z)$ and $F_m(z)$ be single-sided. For double–sided responses, $K-1$ copies of $H_m(z)$, each translated by $\frac{2\pi k}{K}$ radians, cannot exist without overlapping with $F_m(z)$ in their passbands for some values of m, regardless of the value of K.

It is straightforward to show that this filter bank corresponds to a $\frac{M}{K}$-times oversampled generalized DFT (GDFT) filter bank [17] with only the first $M/2$ subband signals retained. For real input signals, the remaining $M/2$ subband signals are complex conjugates of the first $M/2$ signals and are therefore redundant. Thus, without loss of generality, we ignore the subbands $\frac{M}{2} \leq m \leq M-1$.

Since the analysis and synthesis filters have single–sided frequency responses, the time–domain signals after the analysis filters are complex. This necessitates the use of complex arithmetic with any algorithm operating in the subbands.

We now use our conditions on the analysis and synthesis filters to specify the subband components $C_m(z)$ in Figure 1 so that the output of the filter bank $Y_{2R}(z)$ approximates the output $Y_1(z)$ of

[2]With reference to (7), the quantity $A^*(z) = \sum_{n=-\infty}^{\infty} a^*[n]z^{-1}$ for a given sequence $a[n]$.

our model system $S(z)$ of interest. In this vein, the signals $U_m(z^{\frac{1}{K}})$ defined in Figure 1b are given as [1]

$$U_m(z^{\frac{1}{K}}) = \frac{1}{K}\sum_{k=0}^{K-1} H_m(z^{\frac{1}{K}}W_K^k)X(z^{\frac{1}{K}}W_K^k). \tag{10}$$

We can combine the $U_m(z^{\frac{1}{K}})$ into vector form and write

$$\mathbf{u}(z^{\frac{1}{K}}) = \frac{1}{K}\mathbf{H}^T(z^{\frac{1}{K}})\mathbf{x}(z^{\frac{1}{K}}) \tag{11}$$

where $\mathbf{u}(z) = [U_o(z), \ldots, U_{\frac{M}{2}-1}(z)]^T$, $\mathbf{H}(z)$ is the *alias component matrix* given by

$$\mathbf{H}(z) = \begin{bmatrix} H_0(z) & \ldots & \ldots & H_{\frac{M}{2}-1}(z) \\ H_0(zW_K) & \ldots & \ldots & H_{\frac{M}{2}-1}(zW_K) \\ \vdots & & & \vdots \\ H_0(zW_K^{K-1}) & \ldots & \ldots & H_{\frac{M}{2}-1}(zW_K^{K-1}) \end{bmatrix} \tag{12}$$

and the input vector $\mathbf{x}(z) = [X(z), X(zW_K), \ldots, X(zW_K^{K-1})]^T$. The signals $V_m(z)$ after the up-sampler, arranged into the vector $\mathbf{v}(z)$, can then be expressed as

$$\mathbf{v}(z) = \frac{1}{K}\mathbf{C}(z^K)\mathbf{H}^T(z)\mathbf{x}(z). \tag{13}$$

where

$$\mathbf{C}(z^K) = \mathrm{diag}[C_0(z^K), \ldots, C_{\frac{M}{2}-1}(z^K)]. \tag{14}$$

Thus, the filter bank output $Y_2(z)$ can be expressed as

$$Y_2(z) = \frac{1}{K}\mathbf{a}^T(z)\mathbf{x}(z) \tag{15}$$

where

$$\mathbf{a}(z) = \mathbf{H}(z)\mathbf{C}(z^K)\mathbf{f}(z), \tag{16}$$

and

$$\mathbf{f}(z) = [F_0(z), \ldots, F_{\frac{M}{2}-1}(z)]^T. \tag{17}$$

Let us now consider the kth element $a_k(z)$ of $\mathbf{a}(z)$ in (16). It is given as

$$a_k(z) = \sum_{m=0}^{\frac{M}{2}-1} F_m(z)C_m(z^K)H_m(zW_K^k), \quad k = 0, \ldots, K-1. \tag{18}$$

From (6), each set of frequency responses $H_m(zW_K^k)$ and $F_m(z)$ overlap only in their stopbands, for $k \neq 0$. For the time being, we assume an ideal prototype filter. Therefore

$$a_k(z) = 0, \qquad k = 1, \ldots, K-1. \tag{19}$$

Equation (19) is a statement that aliasing error is suppressed in the subbands. From (15) (18) and (19) we then have

$$Y_2(z) = X(z)\frac{1}{K}\sum_{m=0}^{\frac{M}{2}-1} H_m(z)C_m(z^K)F_m(z). \tag{20}$$

We now show that if the $C_m(z^K)$ are chosen to satisfy

$$H_m(z)C_m(z^K) = H_m(z)S(z), \quad m = 0, \ldots, \frac{M}{2} - 1, \tag{21}$$

then $Y_{2R}(z)$ in Figure 1b is equivalent to $Y_1(z)$ in Figure 1a. Accordingly, we substitute (21) into (20) to obtain

$$Y_2(z) = S(z)X(z)\frac{1}{K}\sum_{m=0}^{\frac{M}{2}-1} H_m(z)F_m(z) \tag{22}$$

By taking the real part of the time-domain equivalent $y_2[n]$ of $Y_2(z)$, and recalling that $x[n]$ and $s[n]$ are both pure real, and using (7), we have

$$Y_{2R}(z) = X(z)S(z)\frac{dz^{-k_0}}{K}. \tag{23}$$

Thus $Y_{2R}(z)$ is within a scale and a delay of $Y_1(z)$ as required.

In summary, as a consequence of (6) and (7), with an ideal prototype filter, we see that the filterbank system of Figure 1b with an appropriately chosen *diagonal* system $\mathbf{C}(z)$ inserted between the analysis and synthesis filter banks is indeed equivalent to an arbitrary FIR system $S(z)$. The $C_m(z)$ satisfying (21) are referred to as the *subband components* of $S(z)$.

In the case where the prototype is a non-ideal practical filter whose stopband attenuation is finite, (6) holds only approximately, with the result that (19) to (23) also hold only approximately. The approximations become arbitrarily good as the prototype filter response $H_{pr}(z)$ approaches an ideal characteristic.

We now interpret (21). Since $C_m(e^{jK\omega})$ is periodic with period $\frac{2\pi}{K}$, there are K images in the range $\omega \in [0, 2\pi]$ each of which can have a bandwidth of at most $\frac{2\pi}{K}$. By definition, $C_m(e^{jK\omega})$ is completely specified by one of its periodic images. From (8) the width of Ω_M^m is smaller than (or at most as wide as) the bandwidth of one period of $C(e^{jK\omega})$. This allows us to define the complement of Ω_M^m, $\overline{\Omega_M^m}$, such that $\Omega_M^m \bigcup \overline{\Omega_M^m}$ is a continuous (i.e. non-disjoint) frequency band $\frac{2\pi}{K}$ radians wide and such that $|H_m(e^{j\omega})|$ is negligible for $\omega \in \overline{\Omega_M^m}$. Therefore, $\Omega_M^m \bigcup \overline{\Omega_M^m}$ contains one period of $C(e^{jK\omega})$. Equation (21) restricts the response of $C(e^{jK\omega})$ over Ω_M^m, leaving the response of $C(e^{jK\omega})$ over $\overline{\Omega_M^m}$ arbitrary. The result is that, in general, the subband components $C_m(z)$ corresponding to a full-band response are not unique. Note that $\overline{\Omega_M^m}$ corresponds to the stopband region of the downsampled version of $H_m(z)$. Since $H_m(z)$ and $F_m(z)$ have the same magnitude responses, components of $C_m(e^{jK\omega})$ in $\overline{\Omega_M^m}$ are suppressed by the synthesis filters.

Thus we have the following: in the context of Figure 1 where (6) and (7) are satisfied, then given any FIR scalar system $S(z)$, for each $m \in \left\{0, \ldots, \frac{M}{2} - 1\right\}$ we can find many systems $C_m(z)$ satisfying

$H_m(z)C_m(z^K) = H_m(z)S(z)$. Conversely, if we find many $C_m(z)$ for each $m \in \left\{0, \ldots, \frac{M}{2} - 1\right\}$ whose frequency responses differ only for $\omega \in \overline{\Omega_M^m}$, then each of the $C_m(z)$ (m fixed) will correspond to the same $S(z)$.

We now discuss the computation of the subband components for the case of a practical prototype filter. In this case, it is possible to find FIR subband components $\{C_m(z)\}_{m=0}^{\frac{M}{2}-1}$ such that the system in Figure 1(b) approximates $S(z)$ in a least-squares sense for $z = e^{j\omega}$, when $S(z)$ is FIR. Starting with the approximation (21), downsampling on both sides gives

$$\frac{1}{K}\sum_{k=0}^{K-1} H_m(z^{\frac{1}{K}}W_K^k)C_m(z) \approx \frac{1}{K}\sum_{k=0}^{K-1} H_m(z^{\frac{1}{K}}W_K^k)S(z^{\frac{1}{K}}W_K^k). \tag{24}$$

If aliasing in the subbands is kept small, then a good choice of $C_m(z)$ in this equation will be a good choice of $C_m(z)$ in (21). Define the error in the approximation (24) as

$$E(z) \triangleq \frac{1}{K}\sum_{k=0}^{K-1}\left[H_m(z^{\frac{1}{K}}W_K^k)C_m(z) - H_m(z^{\frac{1}{K}}W_K^k)S(z^{\frac{1}{K}}W_K^k)\right], \tag{25}$$

so that we may find the least-squares approximation for $C_m(z)$ on the unit circle as

$$C_{m,LS}(e^{j\omega}) = \arg\min_{C_m(e^{j\omega})} \frac{1}{2\pi}\int_{-\pi}^{\pi}\left|E(e^{j\omega})\right|^2 d\omega. \tag{26}$$

Using Parseval's equality, this is equivalent in the time-domain to

$$c_{m,LS}[n] = \arg\min_{c_m[n]} \frac{1}{K}\sum_{n\in\mathcal{Z}}\left|h_m[n]_{\downarrow K} * c_m[n] - (h_m[n] * s[n])_{\downarrow K}\right|^2. \tag{27}$$

We define the quantity $\bar{u}_m[n]_{\downarrow K} \triangleq \Big(h_m[n] * s[n]\Big)_{\downarrow K}$ in (27) (where $*$ denotes the convolution operation). This quantity is the time-domain version of $U_m(z^{\frac{1}{K}})$ in Figure 1b, when the input $x[n] = s[n]$. Likewise, we define $\bar{v}_m[n]_{\downarrow K} \triangleq h_m[n]_{\downarrow K} * c_m[n]$. This is the time-domain version of $V_m(z^{\frac{1}{K}})$ when $x[n] = \delta[n]$. Thus, the least-squares solution $c_{m,LS}[n]$ given by (27) is the $c_m[n]$ which forces the corresponding $\bar{v}_m[n]_{\downarrow K}$ to be closest in the least-squares sense to the signal $\bar{u}_m[n]_{\downarrow K}$.

Before solving (27), we consider the length of the subband components $c_m[n]$. We denote L_a to be the length of an associated sequence $a[n]$.[3] (Exceptions are L and N which have already been defined). Then $L_{\bar{u}_m}$, is given by

$$L_{\bar{u}_m} = \left\lceil \frac{L+N-1}{K} \right\rceil, \tag{28}$$

where $\lceil\cdot\rceil$ denotes the ceiling operator, L is the length of $s[n]$ and N is the length of $h_m[n]$. Since we require that $L_{\bar{u}_m} = L_{\bar{v}_m}$, then L_{c_m} is constrained to be

$$\begin{aligned} L_{c_m} &= L_{\bar{u}_m} - L_{h_{\downarrow K}} + 1 \\ &= \left\lceil \frac{L+N-1}{K} \right\rceil - \left\lceil \frac{N}{K} \right\rceil + 1. \end{aligned} \tag{29}$$

[3]For ease of notation, we drop any associated characters "↓" and "[n]"(unless ambiguity arises).

It is important to notice that the length of the subband components is of order $\frac{L}{K}$, which may be significantly smaller than L for large K. Given that the lengths are now established, the coefficients $c_m[n]$ may now be found in a minimum least squares sense of (27) by solving

$$\mathbf{c}_{m,LS} = \arg\min_{\mathbf{c}_m} \|\mathbf{H}_m\mathbf{c}_m - \bar{\mathbf{u}}_{m\downarrow}\|_2^2, \tag{30}$$

where $\mathbf{c}_m = \left[c_m[0], c_m[1], \ldots, c_m[L_{c_m}-1]\right]^T$, $\bar{\mathbf{u}}_{m\downarrow} = \left[\bar{u}_m[0]_{\downarrow K}, \bar{u}_m[1]_{\downarrow K}, \ldots, \bar{u}_m[L_{\bar{u}_m}-1]_{\downarrow K}\right]^T$ and $\mathbf{H}_m$ is the Toeplitz convolution matrix

$$\mathbf{H}_m = \begin{bmatrix} h_m[0] & 0 & 0 & \cdots & 0 \\ h_m[K] & & & & \\ h_m[2K] & & & & \\ \vdots & & & \text{Toeplitz} & \\ h_m[L_{h_{\downarrow K}}-1] & & & & \\ 0 & & & & \\ \vdots & & & & \\ 0 & & & & \end{bmatrix}. \tag{31}$$

Thus, the least-squares subband components of an FIR impulse response $s[n]$ are given by

$$\mathbf{c}_{m,LS} = \mathbf{H}_m^{\#}\bar{\mathbf{u}}_{m\downarrow},\ m = 0, \ldots, \frac{M}{2} - 1, \tag{32}$$

where $\mathbf{H}_m^{\#}$ is the Moore-Penrose pseudo-inverse of the matrix $\mathbf{H}_m$. Since the Moore-Penrose pseudo-inverse is unique for a given full column rank matrix, we can conclude this discussion as follows. Given a full-band system $s[n]$ of length L, a set of $\frac{M}{2}$ FIR analysis filters and synthesis filters of length L satisfying (6) and (7) and downsampling factor satisfying (9), a full-band LTI FIR system $S(z)$ may be approximated in a least-squares sense by a sequence of M in-band filters, $\{C_m(z)\}_{m=0}^{\frac{M}{2}-1}$ of length $\left\lceil\frac{N+L-1}{K}\right\rceil - \left\lceil\frac{N}{K}\right\rceil + 1$.

From (32), we see that the subband component $c_m[n]$ is the deconvolution of the quantity $(s[n] * h_m[n])_{\downarrow K}$ with $h_m[n]_{\downarrow K}$. The overall system response $\hat{s}[n]$ corresponding to a set of subband components $c_{m,s}[n]$ [4] may be computed as

$$\hat{s}[n] = \Re\left[\sum_{m=0}^{\frac{M}{2}-1}\left(h_m[n]_{\downarrow K} * c_{m,s}[n]\right)_{\uparrow K} * f_m[n]\right], \tag{33}$$

which corresponds to the impulse response of Figure 1b.

Even though the development of this section has treated only the case where $S(z)$ is a single–input single–output system, we can extend the development to the multiple–input multiple–output case in a straightforward way. This can be done by incorporating a separate analysis filterbank for each required input, and a separate synthesis filterbank for each required output.

[4] Here, we denote $c_{m,a}[n]$ as the least-squares subband component of some sequence $a[n]$ in the mth subband.

2.2 Properties of the Complex Subband Decomposition

In the following, we assume an ideal prototype filter.

Property 1 *The filter bank structure of Figure 1b is LTI.*

Proof: Using (20), the transfer function $S_R(z) = \frac{Y_{2R}(z)}{X(z)}$ of the filter bank is given by

$$S_R(z) = \frac{1}{K} \sum_{m=0}^{\frac{M}{2}-1} \left[H_m(z) C_m(z^K) F_m(z) + H_m^*(z) C_m^*(z^K) F_m^*(z) \right]. \tag{34}$$

From [18], a system is LTI if and only if it has a transfer function. In the case of a practical prototype filter, extraneous terms appear in (20) which prohibit the definition of a transfer function. However, for a sufficiently good prototype filter, these terms may be considered negligible.

. □

Property 2 *Let $A(z)$ and $B(z)$ be the z-transforms of arbitrary discrete-time signals, and let $C_a(z)$, $C_b(z)$ be the z-transforms of the least-squares subband components of $A(z)$ and $B(z)$ respectively. Furthermore, define $C(z) = A(z)B(z)$ whose least-squares subband components are $C_c(z)$. If for each subband m,*

$$\hat{C}_c(z) \triangleq C_a(z) C_b(z), \tag{35}$$

then

$$H_m(z) \hat{C}_c(z^K) = H_m(z) C_c(z^K). \tag{36}$$

Proof: Since we assume that the stopband attenuation of the analysis filters is perfect, then there exist subband components $C_c(z)$, $C_a(z)$ and $C_b(z)$ for the m-th subband satisfying

$$H_m(z) C_c(z^K) = H_m(z) C(z) \tag{37}$$

$$H_m(z) C_a(z^K) = H_m(z) A(z) \tag{38}$$

$$H_m(z) C_b(z^K) = H_m(z) B(z). \tag{39}$$

Since $C(z) = A(z)B(z)$, from (37) we have

$$\begin{aligned} H_m(z) C_c(z^K) &= H_m(z) C(z) = H_m(z) A(z) B(z) \\ &= H_m(z) C_a(z^K) B(z) = C_a(z^K) H_m(z) B(z) \\ &= C_a(z^K) H_m(z) C_b(z^K) \\ &= H_m(z) C_a(z^K) C_b(z^K) \\ &= H_m(z) \hat{C}_c(z^K). \end{aligned}$$

When there is perfect stopband attenuation, the last equation shows that $C_c(z^K)$ must be equal to $\hat{C}_c(z^K)$ for $z = e^{j\omega}$ only over the frequency range Ω_M^m. For practical filters, these equalities (except for the last one) must be replaced with approximations, giving $H_m(z)C_c(z^K) \approx H_m(z)\hat{C}_c(z^K)$.

. □

This property indicates that we can approximate subband components for a composite system $C(z) = A(z)B(z)$ by convolving the subband components of $A(z)$ and $B(z)$. In general, these subband components are not the least-squares subband components of $C(z)$, but in practice they allow us to approximate the system shown in Figure 4 with that in Figure 5.

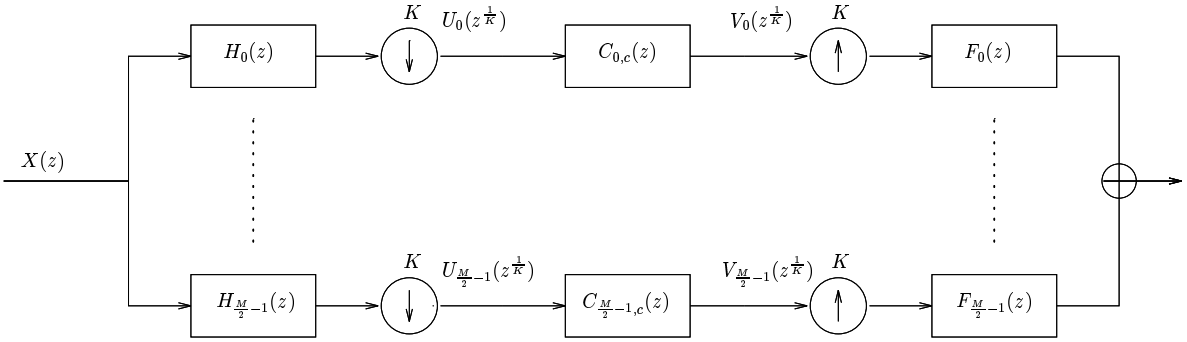

Figure 4: Approximation of $C(z)$ using subband components $C_{m,c}(z)$

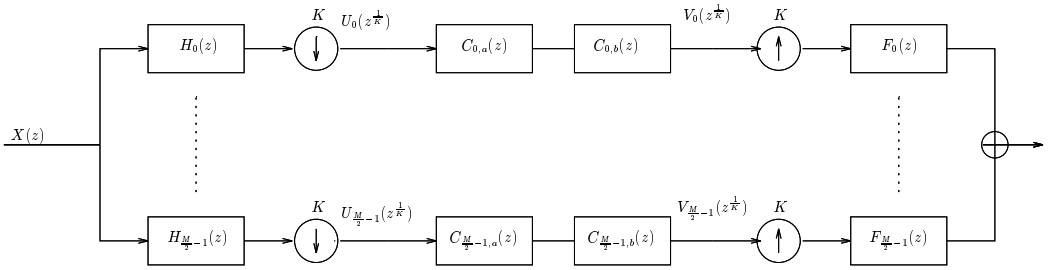

Figure 5: Approximation of $C(z)$ using $C_{m,a}(z)C_{m,b}(z)$.

2.3 Applications to the adaptive filtering problem

We now apply the complex subband decomposition to the adaptive filter problem [21]. The objective is to determine a filter response $g[n]$ to minimize the quantity

$$J \triangleq E(e^2[n]) = E\Big[(x[n] * g[n] - d[n])^2\Big], \tag{40}$$

(or an approximation of J), where $x[n], d[n]$ and $e[n]$ are the input, the desired, and the output error signals respectively. Because any signal can be decomposed into subband components we can

write (40) as

$$J_m \approx E\Big[(c_{m,x*g}[n] - c_{m,d}[n])^2\Big], \qquad m = 0, \ldots, \frac{M}{2} - 1. \tag{41}$$

Using Property 2, we can now write

$$J_m \approx E\Big[(c_{m,e}[n])^2\Big] \tag{42}$$

where

$$c_{m,e}[n] = c_{m,x}[n] * c_{m,g}[n] - c_{m,d}[n]. \tag{43}$$

Equation (42) can be implemented by an adaptive filter algorithm operating inside each subband. (This is the open loop configuration referred to by various authors). Thus, this analysis implies that a subbanded configuration which has an adaptive filter algorithm in each subband yielding a set of subband coefficients $c_{m,g}[n]$ which minimize each J_m in (42) can replace a fullband adaptive filter algorithm whose coefficients $g[n]$ minimize J in (40).

Further, with the commonly-used LMS algorithm, the convergence rate is inversely proportional to the number of taps, L [21]. For a subbanded implementation, the length of the subband components is given from (29) to be $\mathcal{O}(L/K)$. Thus, we expect the convergence rate of the subbanded implementation to improve roughly by a factor of K for this choice of adaptive filter. This is in addition to computational gains which are discussed in Section 4.

In the limit as the filter bank prototype $H_{pr}(z)$ becomes ideal, the subband components given by (43) represent the full band response $e[n]$ exactly. Thus, the error introduced by the subband adaptive filter implementation can become negligible for a good enough specification on $H_{pr}(z)$.

Delayless subband adaptive filtering: The complex subband decomposition leads to a straightforward method of eliminating this filter bank delay. An implementation is shown in Figure 6. Subband components $c_{m,g}[n]$ corresponding to the adaptive filter coefficients are determined by an adaptive filter algorithm operating inside the subbands, as discussed previously. However, the desired output $e[n]$ is computed outside the subbands by convolving the input $x[n]$ with the filter $\hat{g}[n]$, which are the filter coefficients corresponding to the set of subband coefficients $c_{m,g}[n]$, given by (33). The through signal path thus does not experience any delay induced by the analysis or synthesis filter banks. Note that a synthesis filter bank is not required in Figure 6 since the desired output signal $e[n]$ is not computed in the subbands.

This proposed delayless implementation is similar to the open loop configuration of [14], except that our proposed technique uses (33) to update the coefficients, whereas the method of [14] uses a sequence of FFT operations. The development of this technique using the concept of subband components gives the method theoretical rigor and gives new understanding of the approach. The proposed delayless configuration exhibits the same improved convergence performance as the conventional subbanded adaptive filter implementation. However, in the basic form of Figure 6 the delayless structure requires substantially more computations than the conventional subbanded adaptive filter. This is due to the cost of the operation $\hat{g}[n] * x[n]$, which requires L real multiply/adds

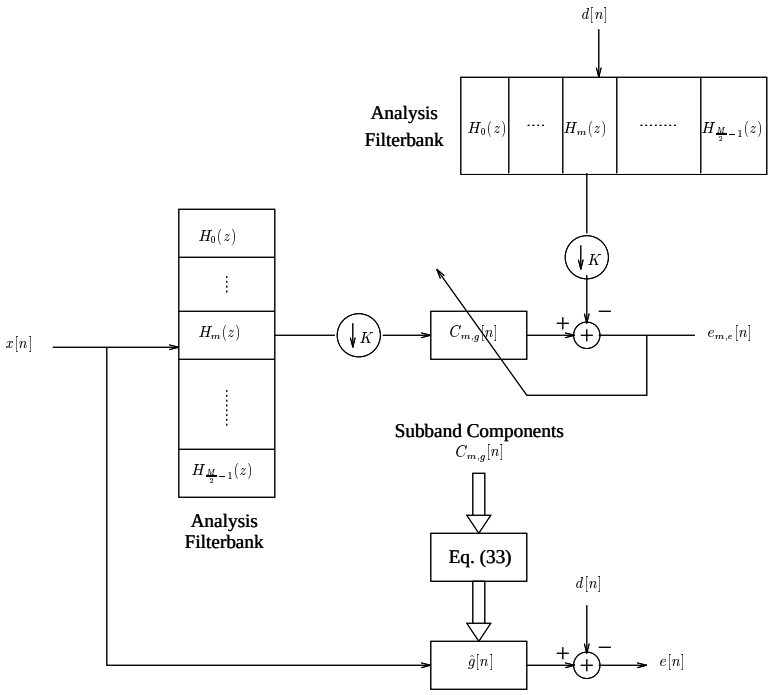

Figure 6: A delayless subbband adaptive filter implementation.

per sample, a figure which can dominate the complexity of the entire configuration. However, in [14], it is shown that the computational cost of this convolution can be reduced by a factor of approximately P, and remain delayless, using a blocked FFT approach. Here, the sequence $\hat{g}[n]$ is partitioned into P segments of equal length. Then the first segment can process by direct convolution (thus giving the delayless property), while the remaining segments process by fast convolutions using FFT's and inverse FFT's, sequentially, for each segment.

Also, additional computational overhead is involved in updating the coefficients $\hat{g}[n]$ according to (33). To save computations, this must be done at periodic intervals, with the effect that the adaptation of the coefficients $\hat{g[n]}$ will lag behind by one period. The expense of this update can be significantly reduced by using a polyphase realization [1] for the filter banks.

3 Filter Design

The design of the filters $H_m(z)$ and $F_m(z)$ for the proposed complex filterbank technique involves fewer constraints than for conventional subbanding systems, since no consideration need be given to cancellation of unwanted aliasing components. There are many design possibilities, since the only requirement is that the $H_m(z)$ and $F_m(z)$ satisfy (6) and (7).

We briefly present two such filter design techniques. The first is based on a spectral factorization of a Nyquist filter. Let N be the length of analysis and synthesis time domain responses $h_m(n)$

and $f_m(n)$ respectively. Let $r(n)$ be a Nyquist response of length $2N+1$. (Any windowed sinc$(\cdot)$ function is a Nyquist response [1]). We interpret the Fourier transform $R(e^{j\omega})$ of $r(n)$ as the magnitude–squared response of the desired prototype filter $H_p(e^{j\omega})$. We can then assign $H_p(e^{j\omega})$ to the minimum–phase spectral factor of $R(e^{j\omega})$. This spectral factorization can be achieved using the complex cepstrum, as outlined in [1], Appendix D. The synthesis filter prototype $F_p(e^{j\omega})$ is assigned to be the paraconjugate of $H_p(e^{j\omega})$. We note in this case, because $R(e^{j\omega})$ is Nyquist, (7) is satisfied with the equality, whereas (6) holds only approximately.

Another approach is a least-squares procedure for designing $H_p(e^{j\omega})$. Here again, we treat $R(e^{j\omega})$, where the corresponding time domain quantity $r(n)$ is of length $2N+1$, as the magnitude-squared response of $H_p(e^{j\omega})$. Consider the objective function Ψ, which involves a criterion on the stop and pass bands, respectively, as follows:

$$\Psi = \lambda \int_{\frac{2\pi}{K}}^{\pi} R(e^{j\omega}) d\omega + (1-\lambda) \int_0^{\frac{\pi}{M}} \left[1 - \sum_{m=0}^{M-1} R(e^{j\omega - \frac{2\pi m}{M}}) \right] d\omega \tag{44}$$

where λ controls the weighting between the stopband and the passband regions. Figure 7 may aid in visualizing the limits on the integral in (44). The sequence $r(n)$ is chosen so that the corresponding $R_{opt}(e^{j\omega})$ is the solution to

$$R_{opt}(e^{j\omega}) = \arg \min_{R(e^{j\omega}) \geq 0} |\Psi| \tag{45}$$

In practice, since the stopband has small magnitude, only the first few terms of the sum in (44) need be considered. By virtue of the constraint in (45), the prototypes $H_p(e^{j\omega})$ and $F_p(e^{j\omega})$ can be calculated by spectral factorization of $R_{opt}(e^{j\omega})$ in the same manner as above.

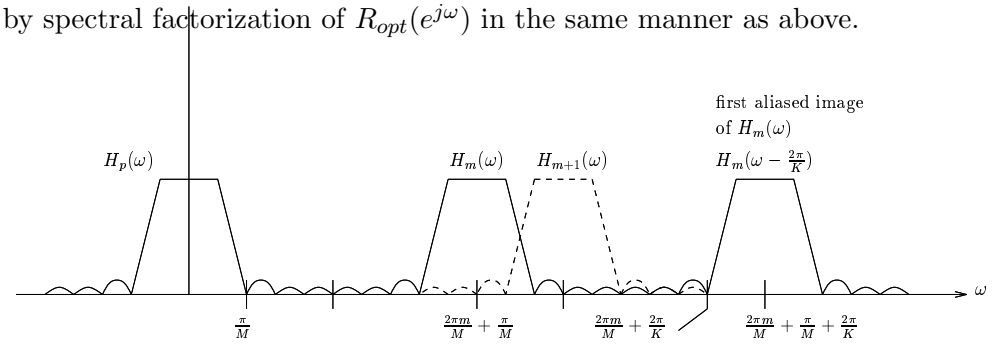

Figure 7: Pertinent frequency values useful for filter design.

An alternative design procedure based on convex optimization of the prototype filter is given in [20].

4 Results

In this section, we present some examples demonstrating the performance of the proposed subbanding technique. First, we present simulations which verify the theoretical development of the

previous sections. We then discuss a subbanded implementation of an acoustic echo canceller (AEC). Next we demonstrate the performance of the delayless subbanded AEC technique. For the following examples, we use a GDFT filter bank with $m_0 = \frac{1}{2}$, $M = 16$ subbands with the upper 8 ignored. The analysis and synthesis filters have $N = 128$ coefficients and are designed to satisfy (6) and (7) well. The magnitude spectra of the analysis filters are shown in Figure 8.

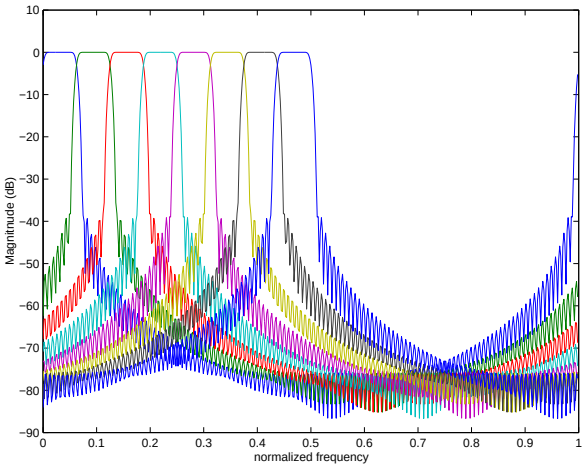

Figure 8: Magnitude Response of 16-Channel GDFT Analysis Filters

4.1 Calculation of the Subband Coefficients

For this example, we decompose an FIR system $s[n]$ with length $L = 100$ into 8 subband components, for variable K. In this example $s[n]$ is a white, zero mean, unit variance Gaussian noise sequence. This experiment demonstrates how well the output signal $y_{2R}[n]$ approximates $y_1[n]$ in Figure 1 versus K when the subband components are calculated using (32), for the given filter bank configuration. The error is calculated as

$$\frac{\sum_n \left| y_{2R}[n] - y_1[n] \right|^2}{\sum_n \left| y_1[n] \right|^2}, \tag{46}$$

expressed in dB. The results are given in Table 1. As can be seen, for only modestly long filters, the approximation can be considered quite accurate.

For the next example, we decompose the same FIR system $s[n]$ above for a fixed $K = 12$, into subband components of length

$$\begin{aligned} & \left\lceil \frac{L+N-1}{K} \right\rceil - \left\lceil \frac{N}{K} \right\rceil + 1 \\ = & \left\lceil \frac{100+127-1}{12} \right\rceil - \left\lceil \frac{127}{12} \right\rceil + 1 = 9. \end{aligned}$$

K	error (dB)
8	-55.97
10	-51.81
12	-42.04
14	-25.51
15	-20.08

Table 1: Approximation error vs. K.

using the the least-squares (LS) approximation given in (32).

Figure 9 shows further results for the fifth subband, which was arbitrarily chosen. The plot in the upper left-hand corner shows the magnitude spectrum of the fifth subband component of $s[n]$, $c_{5,s}[n]$. In the upper right-hand corner, the magnitude spectrum for the downsampled analysis filter (multiplied by K for the sake of appearance) is shown. The lower left-hand plot gives the magnitude spectrum of $\bar{v}_5[n]_{\downarrow K} = (h_5[n] * s[n])_{\downarrow K}$. Finally, the amplitude spectrum of $h_5[n]_{\downarrow K} * c_{5,s}[n]$ is shown in the lower right-hand plot. For comparison, magnitude spectrum of $\bar{v}_5[n]_{\downarrow K}$ is superimposed. As can be seen, the LS subband component allows a good approximation of $v_5[n]_{\downarrow K}$, and the normalized squared error is approximately -43.05 dB.

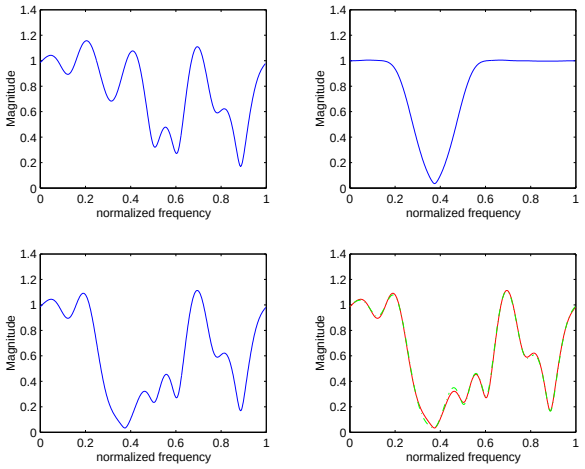

Figure 9: Illustration of LS subband decomposition for $m = 5$.

Now we wish to demonstrate the accuracy of Property 2. For this purpose we use two random sequences $s_0[n]$ and $s_1[n]$, each of length $L = 100$ samples, both similar to that used in the previous section. The real parts of the time domain representation of the signals, corresponding to the $V_m(e^{j\omega})$ in each of Figures 4 and 5 respectively, are shown superimposed in Figure 10, where we have arbitrarily set $m = 5$. The imaginary parts show similar characteristics.

The error due to using $c_{5,s_0}[n] * c_{5,s_1}[n]$ as the subband component of $s_0[n] * s_1[n]$ instead of the

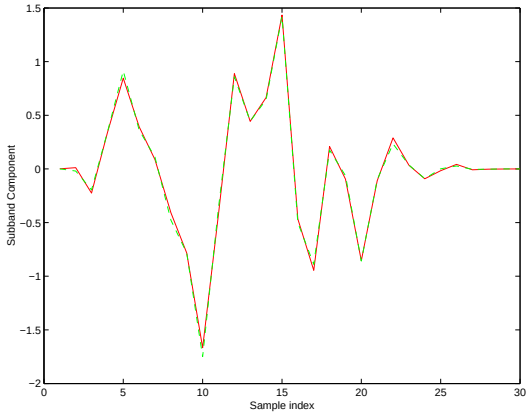

Figure 10: Real Parts of $(h_5[n])_{\downarrow K} * \Big(c_{s_0 * s_1, 5}[n] \Big)$ (solid) and $(h_5[n])_{\downarrow K} * \Big(c_{s_0,5}[n] * c_{s_1,5}[n] \Big)$ (dashed).

least-squares subband component $c_{5,s_0 * s_1}[n]$ is approximately -30.12 dB for this subband. Note that this is the difference in the respective signals $v_5[n]$ in Figures 4 and 5, not the difference in the subband components themselves.

The norm of the difference between the subband component $c_{5,s_0 * s_1}[n]$ and its approximation $c_{5,s_0}[n] * c_{5,s_1}[n]$ (normalized to the norm of $c_{5,s_0 * s_1}[n]$) is -6.76 dB, which is a significant increase over that shown in Figure 10. We see from Figure 11, which shows the two subband components in the frequency domain, that most of this error is concentrated in the region where the magnitude response of $(h_5[n])_{\downarrow K}$ is less significant. This is a direct consequence of the fact that the frequency domain components of any subband component is not specified over $\overline{\Omega_M^m}$, as discussed in Section 2.

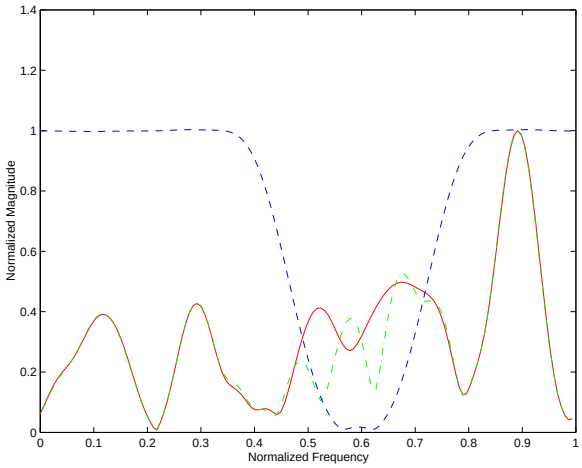

Figure 11: Frequency response of subband component approximations. Solid: Magnitude of the Fourier transform of $c_{5,s_0 * s_1}[n]$, Dot-dashed: Magnitude of the Fourier transform of the approximation $c_{5,s_0}[n] * c_{5,s_1}[n]$. Dashed: Magnitude response of the downsampled analysis filter.

The result is that, when convolving the downsampled analysis filter response with the approximation to the least-squares subband component of $s_0[n] * s_1[n]$, most of the error is suppressed. Since the downsampled synthesis filters have the same magnitude response as the downsampled analysis filters, errors in the subband component approximations are suppressed at the filter bank output as well.

4.2 Application to the AEC problem

We now illustrate the proposed subband decomposition procedure with the acoustic echo cancellation (AEC) problem in telephony [5]–[11], [19]. The AEC problem is depicted in Figure 12, where the objective is to cancel the far-end input speech component which appears at point A in the figure. In this discussion, we do not address the associated double–talk detection problem [22], which has to do with detecting the presence of the near–end speech signal. This example is intended to demonstrate the effectiveness of the proposed complex subbanding scheme in decimating a large adaptive filtering problem into many smaller problems.

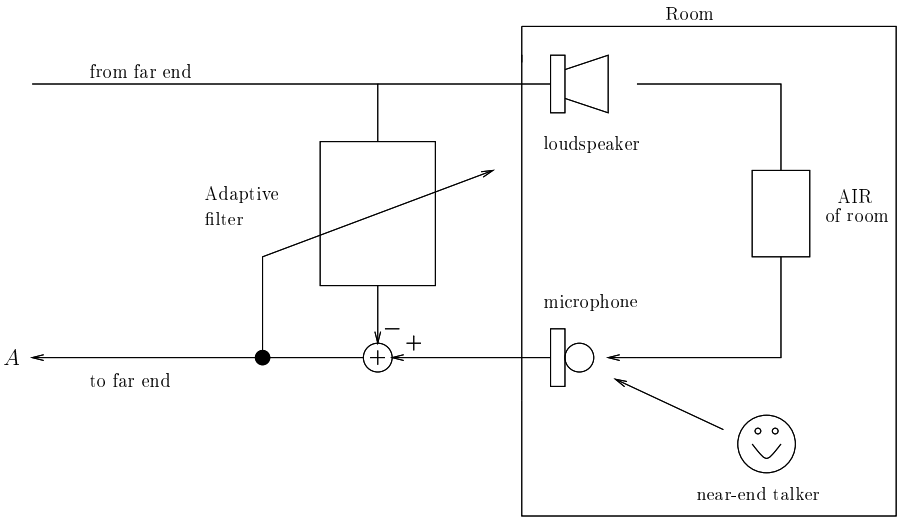

Figure 12: Depiction of the AEC problem.

We demonstrate three cases, each using an acoustic impulse response (AIR), measured in a real room, of 2000 samples in duration at a sampling rate of 8 kHz. The AIR waveform is shown in Figure 13. The input in each case is real speech, approximately 9 seconds in duration. In each case, the echoed speech (that received by the microphone) was generated by convolving the AIR with the input speech signal and is shown in Figure 14. The three test cases correspond to a) the fullband case where no subbanding is used, b) the subbanding method proposed in [5], and c) AEC using the proposed complex subband decomposition. In each case, echo cancellation is achieved using the normalized LMS (NLMS) adaptive filtering algorithm [21], with a value of the NLMS step size parameter $\mu = 0.9$. (For the latter two cases, the NLMS algorithm is applied in each subband

with the error signal being generated in the respective subband). The near–end talker in Figure 12 was silent, and the AIR was assumed stationary over the entire interval. In each case, background noise at an SNR of 25 dB was added to the echo signal.

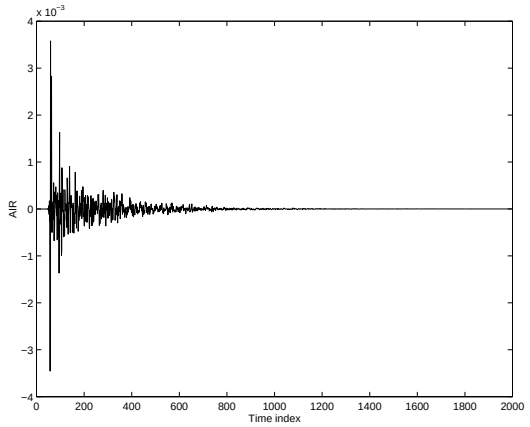

Figure 13: Acoustic impulse response used for AEC example.

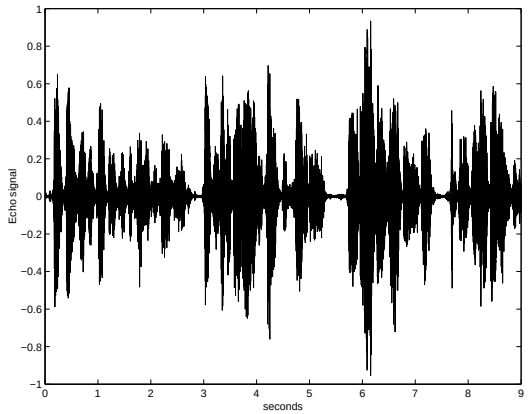

Figure 14: Echoed speech signal for all three echo cancellation experiments.

Results showing echo canceller performance for the fullband echo cancellation case are shown in Figure 15. The top part shows the canceller output vs. time, whereas the bottom part shows echo return loss enhancement (ERLE) in dB. The ERLE is defined as the ratio of the averaged powers after and before cancellation. Lower ERLE implies improved echo cancellation. In each of Figures 15 - 17, power levels have been obtained by averaging the respective signals over a sliding window of 200 samples in duration. It is seen from Figure 15 that the convergence rate for the fullband case is not as fast as desired- just under 6 seconds are required to achieve an ERLE level of -30dB. Further, the computational load is heavier than necessary. It is shown [19] that this configuration requires 32 MIPS[5] at an 8 kHz sampling rate to implement.

[5]MIPS = Millions of Instructions per Second. An instruction includes one real multiply plus one real add.

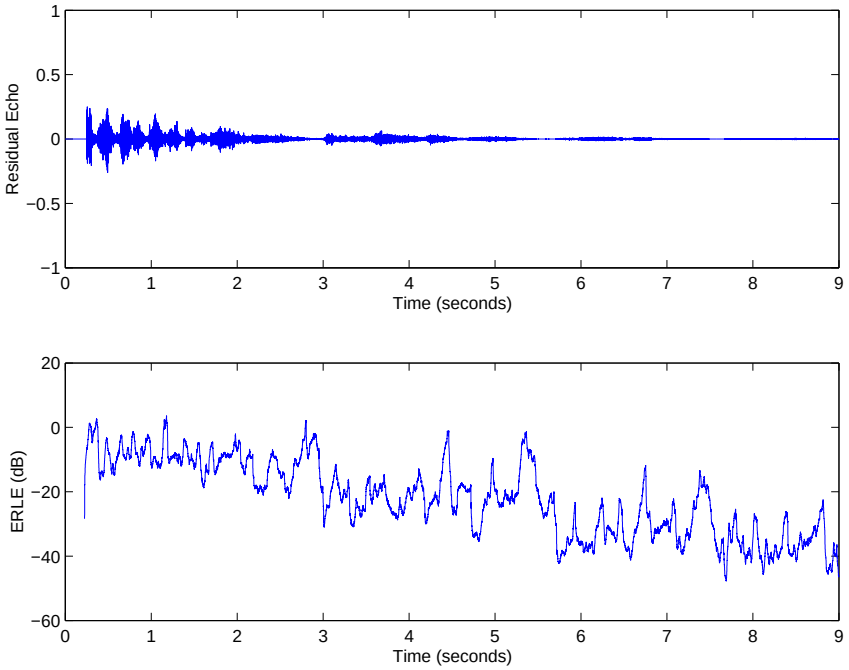

Figure 15: Echo canceller results for the fullband case. Top: residual echo signal vs. time at the canceller output, Bottom: ERLE in dB vs. time.

Simulation results for the method proposed by [5] are shown in Figure 16. This method requires a critically downsampled PR or NPR filterbank with analysis and synthesis filters having conventional double–sided frequency responses. In principle, such a configuration requires a densely–connected $M \times M$ matrix of adaptive filters in the subbands, to completely eliminate aliasing errors at the output. However, in practice, the authors have shown that ideal performance may be closely approximated using only a tridiagonal structure. This implies the adaptive filtering process in each subband requires cross–filters from its adjacent subbands, as well as the adaptive filter in the subband of interest (except of course for the end subbands, which require only one adaptive filter).

The analysis and synthesis filters were generated by cosine modulation of a low–pass quadrature mirror filter prototype, designed according to the method of [1], to yield a PR filterbank. Here, the filter bank coefficients are real, so we define $M' = M/2$. We have used $M' = 8$ and $L = 128$. The results of Figure 16 show that the convergence behaviour of this technique is not significantly improved over the fullband case. This is due to the additional parameters in the cross–filters which must be estimated, thus slowing convergence. Further, the ERLE level obtained using this method is degraded over that obtained with the fullband approach (approximately 22db versus 36dB respectively, over the final one–second epoch). However, this structure does show a significantly improved MIP count over the fullband implementation. It is shown in [19] that this configuration requires 11.7 MIPS for the adaptive filtering operation, and an additional 0.3 MIPS for the filterbank overhead (using a discrete cosine transform implementation), to give a total of 12.0 MIPS. Thus, this

subband configuration offers a substantial saving in computational requirements over the original fullband implementation.

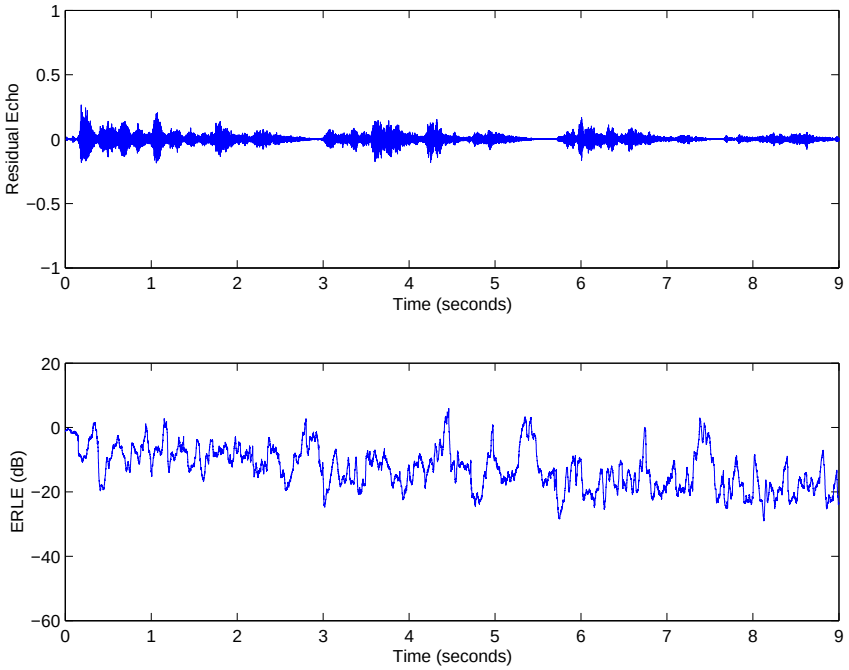

Figure 16: Echo canceller results for the method of [5].

The results using the proposed complex subband decomposition are shown in Figure 17. In this case, we have used a downsampling rate of $K = 0.75M = 12$. Here, we use the same filter bank configuration as in Section 4.1. Because of the diagonal property of the decomposition, we require only one adaptive filter per subband. The significant improvement in convergence speed offered by this approach in comparison to the other two methods is apparent from the figure. A 30dB cancellation level is achieved in just over 3 seconds. However, the point to be emphasized is the reduction in MIP count afforded by the proposed method. Here, the total MIP count is 7.9 [19], including filter bank overhead.

This attractive MIP count figure is achieved despite the penalty of complex arithmetic. This penalty is abated by the use of the higher downsampling rate, and to the fact that only one adaptive filter is required per subband, as opposed to nearly three for the method of [5].

The simulation scenario for the method of [7] is similar to that presented here. The simulation results of [7] indicate roughly equivalent performance as is achieved with the proposed single-sided subbanding scheme.

We therefore observe that proposed single-sided subbanding approach to acoustic echo cancellation offers a competitive alternative to this problem, both in terms of performance and computation. Further, it offers the designer improved flexibility in filter bank design and in the choice of downsampling rates K, an option which is not available with many other methods.

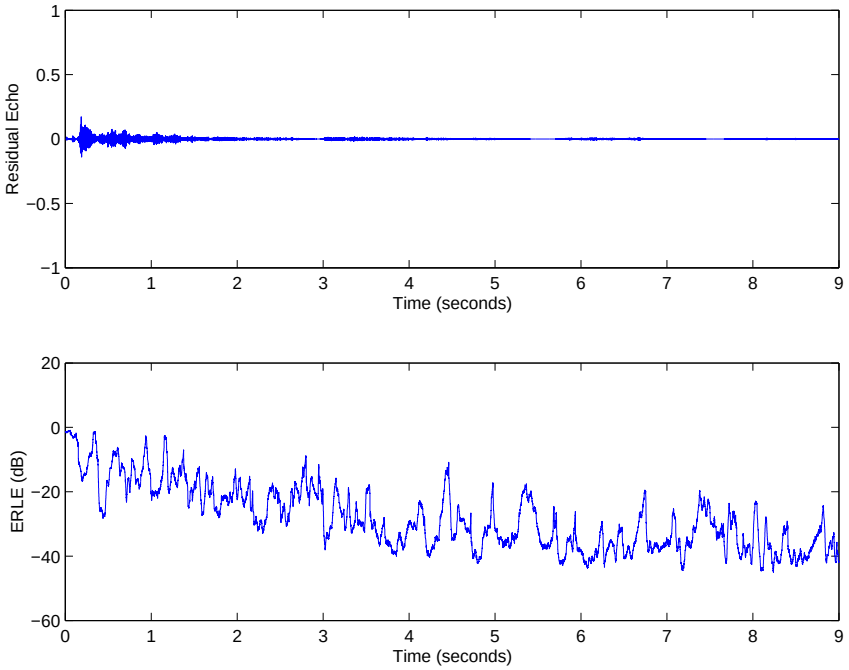

Figure 17: Echo canceller results for the complex subbanding case.

We now demonstrate the performance of the delayless subbanded adaptive filter implementation. The following experiment is identical to the subbanded AEC implementation described above, except the filter coefficients $\hat{g}[n]$ of Figure 6 are computed and updated using (33) from the coefficients inside the subbands every $T = 200$ samples, in the downsampled time scale. Results showing ERLE for both the subbanded and delayless implementations in dB, are shown in Figure 18. Power levels at each time interval are determined by averaging over the previous 200 samples as before. As can be seen, the delayless configuration experiences approximately 5db degradation in suppression performance relative to the subbanded configuration, but nevertheless has a more-than-acceptable level for practical applications. The overall echo suppression level relative to the remote signal level over the entire epoch from 4 to 9 seconds for the subbanded configuration is approximately -30.36dB, and -25.52dB for the delayless configuration.

Implementation Issues: Since we have used uniform DFT filter banks, they can be implemented very efficiently using the polyphase representation, which is discussed at length in [1]. The computational cost for one polyphase filter bank for our purposes is $\frac{4}{K}(L + \frac{M}{4}\log_2 M)$ real multiply/adds per sample (MAPS). Here, we assume that the proposed scheme is to be implemented on a machine which can perform a multiply/add operation in one instruction. In this case, a complex multiply can be configured as four real multiply/add operations. Note that by "sample", we refer to the time scale outside the subbands.

The conventional NLMS algorithm can be implemented in approximately 2ℓ real MAPS, where ℓ is the length of the filter. On this basis, we can compose Table 2 which gives the approximate

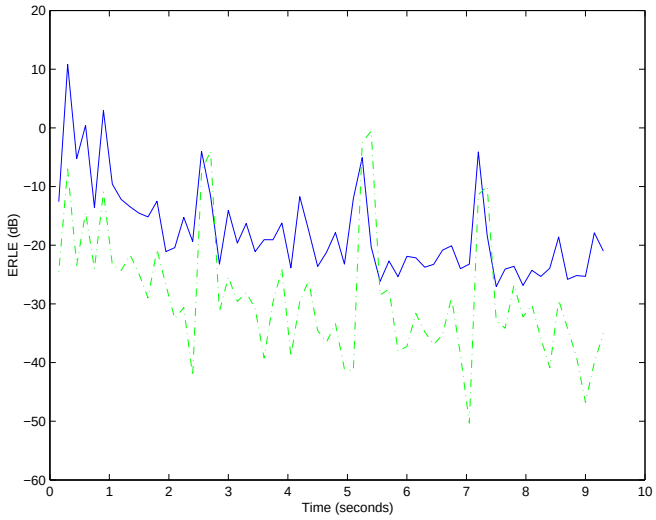

Figure 18: ERLE vs. time. Solid: delayless method, Dashed: subbanded configuration.

Method	**Real MAPS**
Fullband NLMS	$2L$
Method of [5]	$\frac{L}{M'}(6-\frac{1}{M'})+\frac{2}{M'}(N+\frac{M'}{2}\log_2(M'))$
Complex Subband	$4\frac{LM}{K^2}+\frac{8}{K}(N+\frac{M}{4}\log_2 M)$
Delayless	$4\frac{LM}{K^2}+\frac{8}{K}(\frac{T+1}{T})(N+\frac{M}{4}\log_2 M)+3\log_2(Q+1)$

Table 2: Computational complexity of the various implementations.

computational complexity of the various AEC implementations in MAPS, using NLMS in the subbands, including the filter bank overhead (if appropriate).

In Table 2, N is the prototype filter length. Recall the quantity M' in the second row is $M/2$. The last term in the "delayless" expression results from evaluation the fast convolution of $\hat{g}[n]$ with $x[n]$. Here, the filter length L is divided into P blocks of length Q, such that $L = PQ$. FFT's are then performed on each block as discussed in [14]. The filter $\hat{g}[n]$ is updated from its subband coefficients periodically every T samples. To convert the entries in Table 2 to MIPS, we multiply the respective figure by the quantity $f_s/(1 \times 10^6)$, where f_s is the sampling rate at the input (8 kHz for our experiments).

From Table 2, the computational expense and as we have seen earlier the convergence rate, both improve with increasing K. Thus, ideally, we would like to see K as large as possible. However, M must also increase with increasing K, in order to satisfy (9). Since the bandwidth of the prototype filter must then decrease, L also increases so that (6) is satisfied well. This implies more memory for the filter coefficients. This can become a critical issue in applications where cost is important. Thus, K is chosen as a tradeoff between performance and cost. In AEC applications, the choice $M = 8$ appears typical, with the corresponding K set as large as possible.

5 Conclusions

In this paper we have shown that the use of single–sided filter banks leads to near elimination of aliasing error, which in turn permits a *diagonal* decomposition of a broad class of large problems into smaller, more tractable pieces. The application of filter bank theory is therefore significantly expanded. We have shown there exists a many–to–one correspondence between the set of subband components and the model response of interest, and that there exists an equivalence between convolution outside the subbands and convolution inside the subbands. The filter bank design process is simplified over conventional methods since the filters are not constrained by the need to cancel aliasing errors. The downsampling rate for a fixed filterbank is variable, up to the number of subbands for ideal filter responses. These results lead to new insights into the way signal processing algorithms can be implemented.

The method has been verified using the acoustic echo cancellation (AEC) problem. Performance of the single–sided subbanding technique has been shown to exceed or meet that of previous AEC methods, both with respect to convergence and with respect to computational requirements. The complex subband decomposition leads naturally to a delayless AEC implementation, whose performance has been verified to be almost equivalent to the conventional subbanded implementation.

6 Acknowledgments

The authors wish to acknowledge and thank the following institutions for their support of this project: Mitel Corporation, Kanata, Ontario, Canada; The Centre for Information Technology Ontario (CITO); and the Natural Sciences and Engineering Research Council of Canada (NSERC).

References

[1] P. P. Vaidyanathan, "Multirate systems and filter banks", Prentice Hall, New Jersey, 1993.

[2] B. W. Gillespie, R. S. Malver, and D. A. F. Florencio, "Speech dereverberation via maximum–kurtosis subband adaptive filtering", *ICASSP2001*, May, 2001, Salt Lake City, U.S.A.

[3] W. Kellerman, "Strategies for combining acoustic echo cancellation and adaptive beamforming microphone arrays", Proc. *ICASSP97*, April 1997, Munich, Germany.

[4] S. J. Elliot, I. M. Stothers, and P. A. Nelson, "A multiple error LMS algorithm and its application to the active control of sound and vibration", *IEEE Trans. Acoust. Speech and Signal Processing*, Vol. ASSP–35, Oct. 1987, pp. 1423–1434.

[5] A. Gilliore and M. Vetterli, "Adaptive filtering in subbands with critical sampling", *IEEE Trans. Sig. Proc.*, Aug. 1992, pp. 1862-1875.

[6] Q. Jin, Z-Q. Luo, and K. M. Wong, "Optimum filter banks for signal decompositions and its application in Adaptive Echo Cancellation", *IEEE Trans. Sig. Proc.*, July 1996, pp. 1669-1679.

[7] S. S. Pradhan and V. U. Reddy, "A new approach to subband adaptive filtering", *IEEE Trans. Sig. Proc.* Mar. 1999, pp. 655-664.

[8] J. Reilly, M. Seibert, N. Ahmadvand, and G. Reesor, "Single–sided filters with application to Acoustic Echo Cancellation", Patent Application, submitted August 1998.

[9] J. Reilly, M. Seibert, M. Wilbur and N. Ahmadvand, "The decomposition of large problems using single-sided subbanding", *ICASSP2000*, June 2000, Istanbul, Turkey.

[10] S. Weiss, M. Hartneck and R. W. Stewart, "Design of near perfect reconstruction oversampled filter banks for subband adaptive filters", *IEEE Trans. Circ. Syst. II*, Aug. 1999, pp. 1081-1085.

[11] W. H. Chin and B. Farhang–Boroujeny, "Subband adaptive filtering with real–valued subband signals for acoustic echo cancellation", *IEE. Proc. Vis. Image Signal Process.* Vol. 148, No. 4, August 2001, pp. 283-288.

[12] M. Thomlinson and K. M. Wong, "Techniques for the digital interfacing of t.d.m.–f.d.m. systems", *Proc. IEE*, Vol. 123, No. 12, December, 1976, pp. 1285-1292.

[13] M. G. Bellanger, J. L. Daguet, G. P. Lepagnoi, "Interpolation, extrapolation, and reduction of computation speed in digital filters", *IEEE Trans. ASSP*, Vol. ASSP-22, Aug. 1974, pp. 231-235.

[14] D. R. Morgan and J. C. Thi, "A delayless subband adaptive filter architecture", *IEEE Trans. Signal Processing*, Vol. 43, No. 8, August 1995, pp.1819–1830.

[15] R. Merched, P. S. R. Diniz, M. R. Petralia, "A new delayless subband adaptive filter structure", *IEEE Trans. Signal Processing*, Vol. 47, No. 6, June 1999, pp. 1580–1591.

[16] Y. Bendel, D. Burshtein, O. Shalvi, and E. Weinstein, "Delayless frequency domain acoustic echo cancellation", *IEEE Trans. Signal Processing,* Vol. 9, No. 5, July 2001, pp. 589–597.

[17] R. E. Crochiere and L. R. Rabiner, "Multirate Digital Signal Processing", Prentice–Hall Inc., Englewood Cliffs, New Jersey, 1983.

[18] T. Kailath, "Linear Systems", Prentice–Hall Inc., Englewood Cliffs, New Jersey, 1980.

[19] M. T. Seibert, "Acoustic echo cancellation using single–sided subbanding" M.Eng Thesis, Dept. of Elect. and Comp. Eng., McMaster University, Hamilton, Ontario, Canada, October, 1999.

[20] M. Wilbur, "Application of subbanding methods to the decimation of large problems", M.Eng. Theis, Dept. of Elect. and Comp. Eng., McMaster University, Hamilton, Ontario, Canada, June, 2000.

[21] S. Haykin, "Adaptive Filter Theory", Prentice Hall, Englewood Cliffs, New Jersey, 3rd Ed,. 1996.

[22] H. Cho, D. R. Morgan, and Jacob Benesty, "An objective technique for evaluating doubletalk detectors in acoustic echo cancelers", *IEEE Trans. Speech and Audio Processing*, Vol. 7, No.6, Nov. 1999, pp. 718-724.